J Mater Sci: Mater Med (2007) 18:779–786
DOI 10.1007/s10856-006-0007-z

Synthesis, corrosion and wear of anodic oxide coatings on Ti–6Al–4V

R. Narayanan · Partho Mukherjee · S. K. Seshadri

Received: 24 August 2005 / Accepted: 8 December 2005 / Published online: 2 December 2006

Abstract Electrodeposited anodic oxide coatings were produced on Ti–6Al–4V substrates using aqueous electrolytes containing dissolved calcium and phosphorus. Different coatings were produced by varying the time periods. The coatings were characterised by XRD technique and TEM. The coatings were exposed to Simulated Body Fluid (SBF). Electrochemical polarisation and ac impedance studies too were performed on the coatings in SBF. Pins were coated and run against wooden disc in pin-on-disc type of wear tests. Coatings produced from long time electrolysis showed very good resistance to the attack of SBF and less wear compared to those produced from short time exposure.

1 Introduction

Titanium and its alloys are the materials of choice for most dental and orthopaedic applications [1] They have excellent corrosion resistance and good compatibility with bone and are widely used as implant materials [2-4] A stable and thin oxide layer formed naturally on the surface offers high degree of biocompatibility of titanium alloys [5]

Of the various alloys of titanium, Ti–6Al–4V is commonly used for orthopaedic implants. However, Al and V are released from the implant surface to the body and the presence of even a small amount of these may cause local irritation of tissues surrounding the implant [3].

Bone response and implant success depend on the properties of the surface [1]. To overcome the problem of ion release and improve the surface characteristics for better bone bonding, many surface treatment techniques like anodic oxidation [3, 6, 7], sol–gel method [8], electrophoretic deposition [9] and ion implantation [10] are used. Among these treatments, anodic oxidation is a superior and inexpensive method. It can result in rough and porous surfaces [2] and uniform coatings at ambient temperatures [3]. It can also incorporate chemical elements from the electrolyte in order to improve protective properties [7].

This paper describes an anodic oxidation method of synthesising titanium oxide coatings on Ti–6Al–4V substrates and evaluating their structural features as well as corrosion and wear properties. The electrolytic solutions used were made up of calcium and phosphorus compounds dissolved in water.

2 Experimental procedure

The electrolyte used in this work contains 0.15 M/l of calcium acetate (CA) and 0.01 M/l of β-sodium glycero phosphate (β-GP) in water. This solution has a molar ratio of (CA) to (β-GP) as 15 [11] while Ca/P weight ratio was 19.3. The pH of the solution was 7.6.

Rectangular samples of Ti–6Al–4V of area 2×3 cm^2 were used as anode. Stainless steel plate was used as cathode to complete the electrolytic cell. The coatings were obtained by applying a current

R. Narayanan (✉) · P. Mukherjee · S. K. Seshadri
Department of Metallurgical and Materials Engineering, Indian Institute of Technology, Chennai (Madras) 600 036, India
e-mail: rnarayan69@hotmail.com

density of 10 mA/cm^2 (corresponding to a voltage of 30 V maximum). The operations involved in the coating process were in the following sequence: (a) mechanical polishing (b) etching in a solution containing 1 part HF, 4 parts HNO_3 and 5 parts H_2O (c) anodising in the electrolytic solution at 10 mA/cm^2 for 15 min, 45 min, 3, 6, 10, 20 and 24 h. Philips (Model XD-D1) microprocessor controlled X-ray diffractometer was used to identify the various phases using CuKα incident radiation (λ = 1.5481 Å). XRF method was used to obtain the chemical composition of the coatings.

Philips (Model CM 12 STEM Unit) TEM using electron energy of 120 kV, was used to obtain the minute coating features and nature of crystallinity. Porosity measurements were made using image analyser attached to Leitz Laborlux 12ME microscope. Thickness measurements were made using Gaertner ellipsometer (Model 119 XVV) employing He–Ne laser of wavelength 632.8 nm and using Frenel's formula. Surface roughness of the coatings was measured using Mahr (M2) Perthometer and employing a traverse length of 17.5 mm.

The coatings were immersed for a period of 1 month in a buffered physiological solution [6], containing NaCl 8.74 g/l, $NaHCO_3$ 0.35 g/l, Na_2HPO_4 0.06 g/l and NaH_2PO_4 0.06 g/l. The pH of the solution was 7.4. Loss of weight of the coatings is taken as a measure of the loss of elements from the coatings to the solution. Electrochemical polarisation of the coatings was carried out using microprocessor controlled ACM corrosion testing unit. The coating formed the working electrode and graphite formed the auxiliary electrode. Polarisation was carried out in the range –700 to 4000 mV (vs. SCE) at a scan rate of 300 mV/min. Impedance test was conducted in the frequency range 10^4 to 10^{-2} Hz.

Pin-on-disc type of wear tests were done to elucidate the friction and wear behaviour of coatings. Ti–6Al–4V pins of diameter 10 mm and height 30 mm were coated at the ends. Wooden discs of dia 50 mm and thickness 6 mm which resemble cortical bone in terms of hardness and elastic modulus [12] were used for wearing out the coated pins. Before the tests were performed, coated pins were weighed. Diameter of the run-track was 30 mm and speed was 50 rpm. Tests were conducted for 50 min. During the running of the tests, co-efficients of friction were continuously recorded. After the wear tests were over, wear debris was carefully removed using acetone and weights measured. The weight difference gives the amount of coating lost during the wear test. This is used to calculate the specific wear rate.

3 Results and discussion

Nomenclature and chemical composition of the coatings is given in Table 1. The coatings were produced by anodic oxidation and contained calcium and therefore, are referred to as ''AC...''. With increasing time, both calcium and phosphorus from the solution deposit in more quantities in the coating. This could be because of higher retention time of both calcium and phosphorus at the coating surface, which enables better adsorption.

4 Structural features

All the coatings contained TiO where titanium is present in divalent state. It is significant that the coating does not contain aluminium oxide. Presence of calcium and phosphorus is not detected by normal angle XRD (Fig. 1). It can be seen from Pourbaix pH-potential diagram [13] that, for titanium–H_2O system, TiO is the predominant phase at lower potentials and TiO_2 at higher potentials, in the pH range 6–7. Thus, it can be surmised that applied voltage of upto 30 V used in this study, is not high enough to form the higher oxide TiO_2.

Details of TEM for coatings AC1, AC4 and AC7 are given in Figs. 2, 3, 4 and Table 2 gives the phases identified by TEM. Figures 2, 3 show the amorphous character of the coatings AC1 and AC4. Both coatings show amorphous character in electron diffraction; however, crystalline peaks corresponding to TiO appear in X-ray diffraction. It has been reported in an earlier work that TEM analysis of anodic titanium oxide showed amorphous character [14, 15], although XRD analysis of the same sample showed crystalline peaks [15]. XRD uses a larger surface area for inspection and hence, more crystalline area contributes to the diffraction pattern. While TEM studies use a very thin sample with a very small surface area and so, many crystals even if present may not contribute to

Table 1 Nomenclature and chemical composition of the coatings

Coating time	Nomenclature	Chemical composition	
		% Ca	% P
15 min	AC1	0.04	0.05
30 min	AC2	0.04	0.07
3 h	AC3	0.08	0.11
6 h	AC4	0.28	1.31
10 h	AC5	0.27	1.29
20 h	AC6	0.30	1.16
24 h	AC7	0.38	1.22

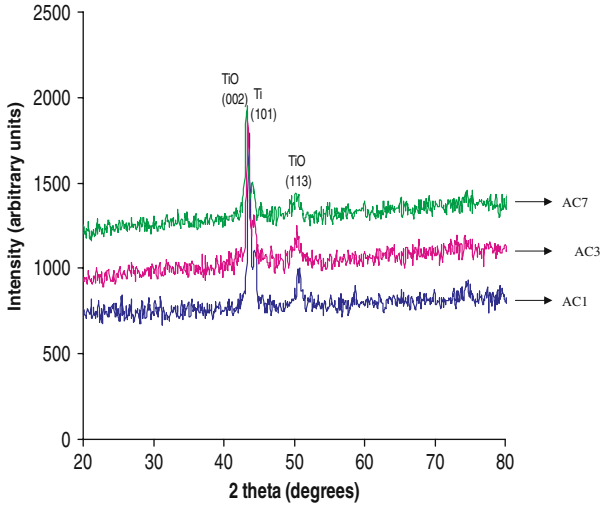

Fig. 1 XRD pattern of coatings

diffraction pattern. This difference manifests as change in the diffraction pattern observed by TEM. Sample AC7 is coated for sufficiently long time; this helps in enhanced crystallisation. This is indicated by the diffraction pattern (Fig. 4a) and the grain structure (Fig. 4b).

Table 3 gives the thickness, porosity and roughness of the coatings. If the coating time is short (15 min) thickness is small. And if the coating time is large (10, 20 and 24 h) coating thickness is again small. Thicker coatings were obtained when the coating is carried out for 45 min and 3 h. It is seen that, 171 nm is the maximum value achieved in the present study.

Short deposition time (15 min) results in amorphous structure and a thin coating. Longer deposition times, however, result in poor adhesion of oxide layer with the substrate. This results in spalling-off of the deposit and formation of a thin coating.

Figure 5 gives the details of the pores formed during coating. The anodic oxidation process itself occurs by dissolution and re-deposition of the oxide. If the dissolution reaction is faster than the deposition reaction, formation of pores is favoured. On the contrary, if deposition mechanism predominates over the dissolution reaction, then pore formation is less favoured.

Short coating time (15 min) does not allow adequate time for dissolution and hence, only small pores are formed. Very high coating duration (20 and 24 h) allow for deposition mechanism to predominate over the dissolution mechanism leading to fewer and smaller pores.

Coatings AC1 (Fig. 5a) and AC3 have larger pores and coating AC4 (Fig. 5b) has the largest pore. Long-time coatings AC6 and AC7 (Fig. 5c, d, respectively) have few small-sized pores.

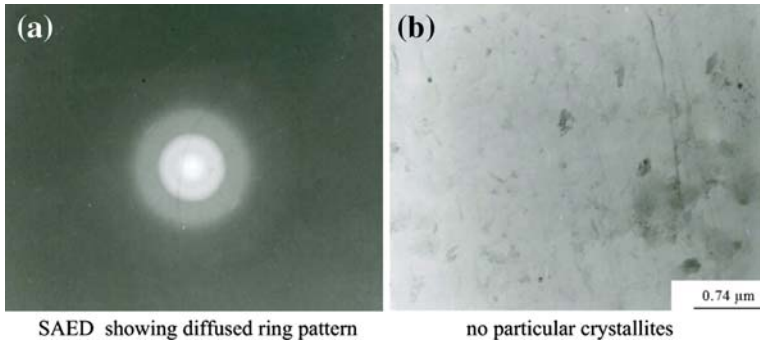

Fig. 2 TEM of AC1. (a) SAED showing diffused ring pattern; (b) no particular crystallites

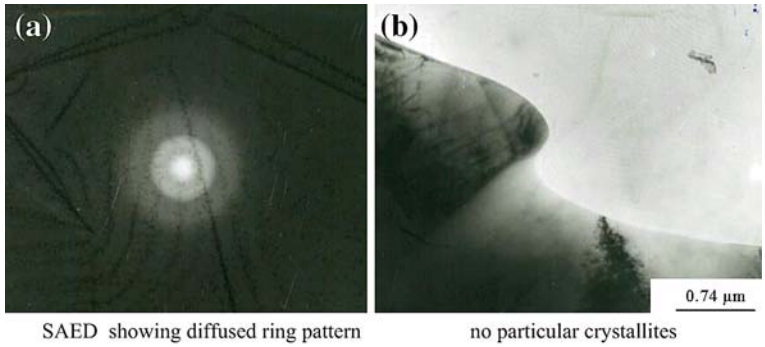

Fig. 3 TEM of AC4. (a) SAED showing diffused ring pattern; (b) no particular crystallites

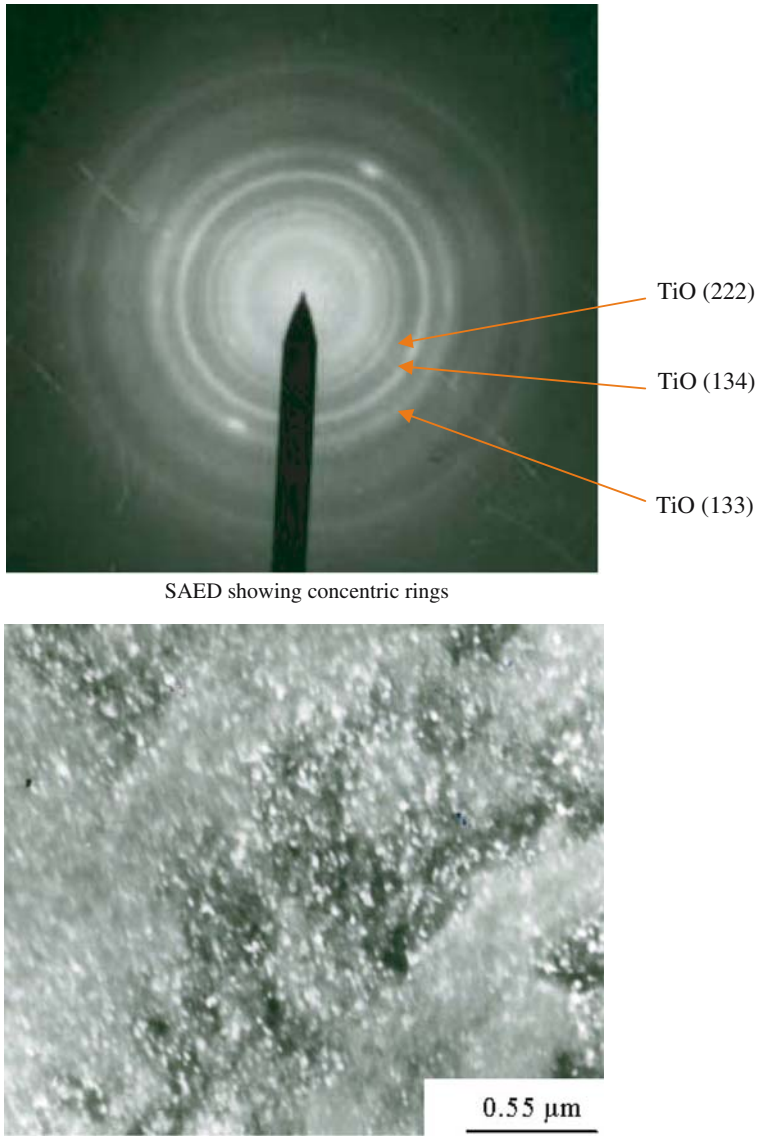

Fig. 4 TEM of AC7. (a) SAED showing concentric rings; (b) structure showing crystallites

Coatings AC1, AC2, AC3 and AC5 have smooth surface while coatings AC6 and AC7 have rough surface. This observation will be useful in discussion about the nature of debris during wear characteristics.

Table 2 TEM results

Coating	Camera constant $L\ \lambda$ (Å mm) (length = 155 mm)	R (mm)	D (Å) = $L\lambda/R$	Phases
AC1	5.19	Amorphous	–	
AC4	5.19	Amorphous	–	
AC7	5.19	3.47	1.49	TiO (222)
	5.19	4.54	1.14	TiO (134)
	5.19	5.63	0.92	TiO (133)

5 Corrosion in SBF

Corrosion of the coatings is influenced by several parameters, the most important being thickness, calcium content and porosity. Presence of self-healing

Table 3 Thickness and porosity of the coatings

Coating	Thickness (nm)	Size of large pore (microns)	Roughness (R_a) (μm)
AC1	110	30	0.291
AC2	170	52	0.301
AC3	171	54	0.305
AC4	116	77	1.69
AC5	119	50	0.253
AC6	120	16	1.68
AC7	107	9	2.716

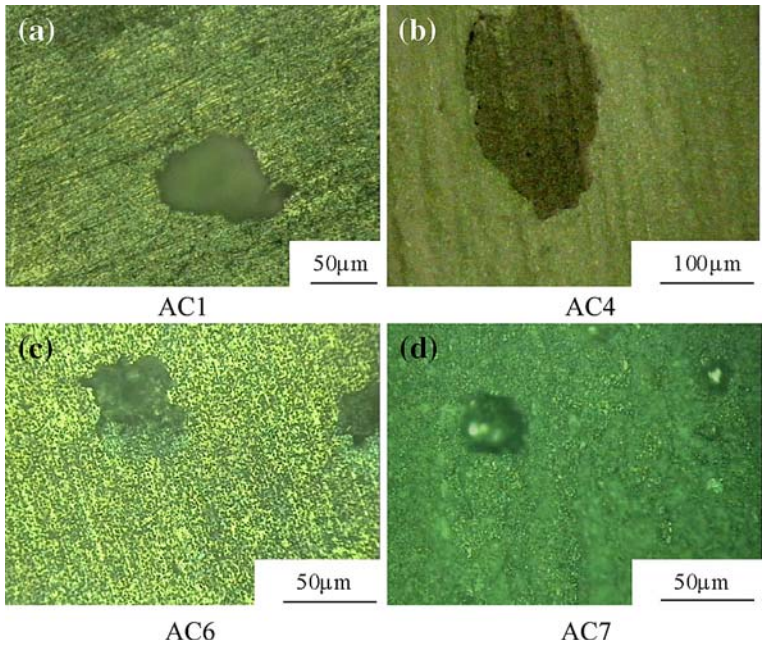

Fig. 5 Pores in the coatings. (a) AC1, (b) AC4, (c) AC6, (d) AC7

pores, lower calcium content, higher phosphorus content and high thickness tend to increase the corrosion resistance of the coatings.

Figure 6 gives the corrosion rate expressed in milligram/sq. decimeter/day (mdd) of the coatings exposed to SBF for 1 month. The coatings were subjected to uniform corrosion. After prolonged exposure, the porous oxide may become hydrated and ions may get incorporated easily into the pores leading to further precipitation [16] and resulting in either corrosion or self-healing. The porous oxide coating produced in this work (AC4) is self-healing, as is evidenced by slightly lower corrosion rate (Fig. 6). Amorphous coatings AC1 and AC4 show very good corrosion resistance. The coating AC7 is less porous and hence shows high corrosion rate probably because of the absence of self-healing effect.

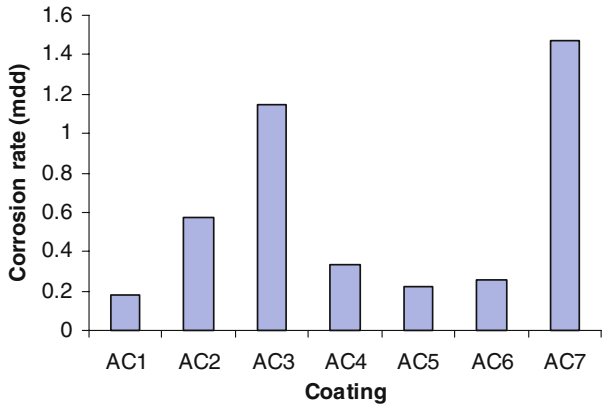

Fig. 6 Corrosion of the coatings after exposure to SBF for 1 month

Tables 4, 5 give the results of potentiodynamic polarisation and ac impedance, respectively. An equivalent circuit modelling the corrosion behaviour during the application of ac signal is given in Fig. 7. The circuit consists of one R–C element connected in series with a Warburg element and connected in parallel with a constant phase element. The constant phase element (CPE) corresponds to the electronic transfer at the interface dominated by porous nature of the oxide film and is the impedance provided by the roughness and inhomogenity of the porous and passive layers. The lower branch of the circuit, namely, Warburg impedance accounts for the Faradaic process, namely, transfer of ions across the coating (porous and passive layers) [17].

Of all the coatings, AC1, AC4 and AC5 show lower corrosion current and they do not passivate. Though AC1 shows lower corrosion current, its impedance is low because of its lower thickness. AC2 and AC3 have similar thickness and pore size, but different calcium levels. AC3 which has higher calcium among these two coatings, shows inferior resistance to corrosion. AC4 and AC5 have high phosphorus content which will improve corrosion resistance. However, AC5 has larger self-healing pores than AC4 and hence its corrosion resistance is higher than that of AC4. AC6 and AC7 have lower thickness and offer poor resistance to the attack by SBF.

It has been shown that passive current density for anodic oxide on Ti–6Al–4V in SBF is 0.05 $\mu A/cm^2$ [18] and the oxide Al_2O_3 present in the coating offers resistance to attack by SBF [19]. Coatings produced in

Table 4 Tafel plot results

Coating	i_{corr} (μA/cm^2)	i_{pas} (μA/cm^2)	Range of passivation (mV)
AC1	0.32	No passivation	No passivation
AC2	0.58	No passivation	No passivation
AC3	1.64	No passivation	No passivation
AC4	0.39	No passivation	No passivation
AC5	0.31	No passivation	No passivation
AC6	0.62	7.5	900–1900
AC7	4.6	No passivation	No passivation

Table 5 Results of ac impedance

Coating	Roughness factor (n)	CPE (ohm)	Warburg impedance (ohm)	R_{ct} (ohm)	C_{dl} (F)	Total impedance (ohm cm^2)
AC1	0.78	109.05	92.1×10^5	129×10^6	2.37×10^3	109
AC2	0.837	6.62	18.1×10^5	32.2×10^6	1.53×10^3	6.6
AC3	0.764	125	814×10^5	0.4×10^6	1.52×10^3	125
AC4	0.571	6822	8.68×10^5	430×10^6	2.25×10^3	6822
AC5	0.53	9960	33.7×10^5	6.14×10^6	2.19×10^3	9960
AC6	0.74	1560	5.54×10^5	43×10^6	2.18×10^3	1560
AC7	0.917	3.28	17.7×10^5	0.072×10^6	2.43×10^3	3.28

this work did not contain Al_2O_3 and this could be the reason why the corrosion current densities reported in this work are higher than 0.05 μA/cm^2. Comparison of corrosion current densities of anodic oxides on titanium alloys with and without vanadium shows slightly lower corrosion rates for the alloys without vanadium [20]. It is possible that the same oxide coatings produced on titanium alloys not containing any vanadium show lower corrosion currents than reported in this paper.

A combination of higher thickness, presence of large-sized self-healing pores, lower calcium contents and larger amounts of phosphorus will increase the resistance of the coatings to the attack by SBF.

Coatings AC4 and AC5 have large pores, have low corrosion currents and show high impedance. It is expected that increasing pore size increases corrosion rate in SBF because of higher probability of exchange of ions through the pores. But the larger pores in the coatings AC4 and AC5 actually may become hydrated and ions may easily be incorporated into the pores and further precipitated, as described earlier. When the pores are filled by hydrated or precipitated compounds, the thickened oxide film can become highly self-protective again, i.e., oxide film is self-healed [16]. Thus, larger pores in coating AC5 are beneficial in their ability to form hydrated compounds and reduce the attack by SBF.

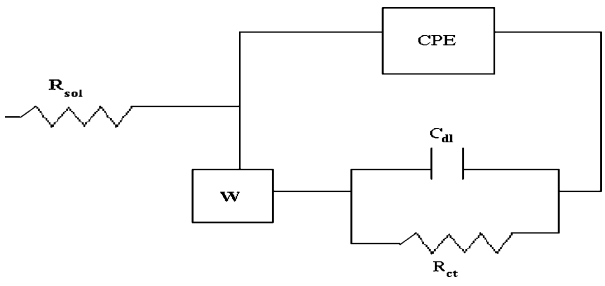

Fig. 7 Equivalent circuit depicting the corrosion model

6 Pin-on-disc wear

An earlier work has reported [12] the use of wooden disc to test the wear of hydroxy apatite coatings. In a similar approach, wooden discs have been used to run against coatings produced on Ti–6Al–4V pins. Figures 8, 9, 10, 11 show the wear tracks and values of friction co-efficient produced in these tests. Table 6 gives the specific wear rates of these coatings.

All the coatings contained scoring marks which are indicative of mild abrasive wear. No adhesion of coating material was seen on the wooden surface. Black debris was smeared throughout the wear track on the wooden disc. Co-efficients of friction of the coatings were below 0.20. Coatings produced from longer exposure times (AC6, AC7) have rough surface (Table 3) but lower specific wear rate (Table 6). Coatings AC1, AC2 and AC3 have smooth surface (Table 3) but higher specific wear rate (Table 6).

Smooth surfaces result in poor bony adhesion and are predominantly anchored by soft tissue, while rough

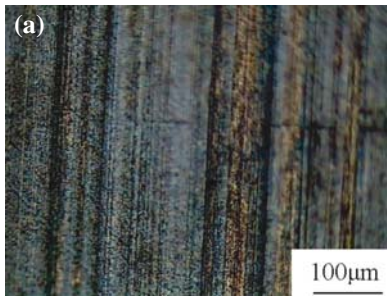

Wear track after running against wooden disc for 50 minutes

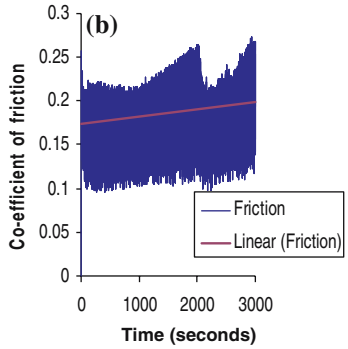

Variation of co-efficient of friction with time

Fig. 8 Wear characteristics of AC1 without SBF. (a) Wear track running against wooden disc for 50 min. (b) Variation of co-efficient of friction with time

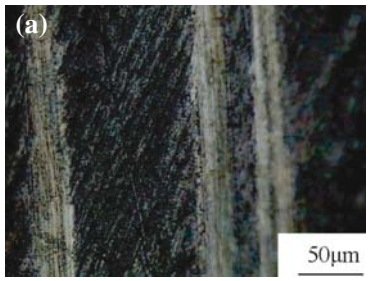

Wear track after running against wooden disc for 50 minutes

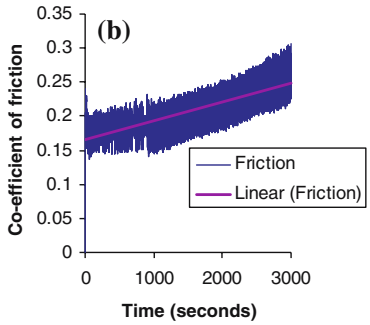

Variation of co-efficient of friction with time

Fig. 9 Wear characteristics of AC3 without SBF. (a) Wear track running against wooden disc for 50 min. (b) Variation of co-efficient of friction with time

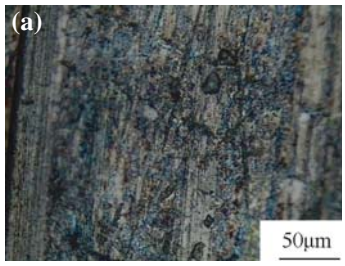

Wear track after running against wooden disc for 50 minutes

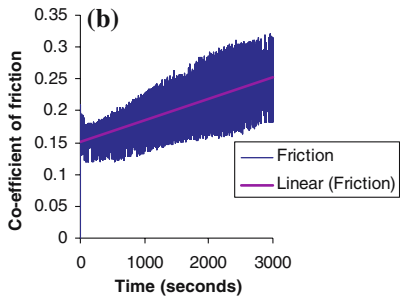

Variation of co-efficient of friction with time

Fig. 10 Wear characteristics of AC5 without SBF. (a) Wear track running against wooden disc for 50 min. (b) Variation of co-efficient of friction with time

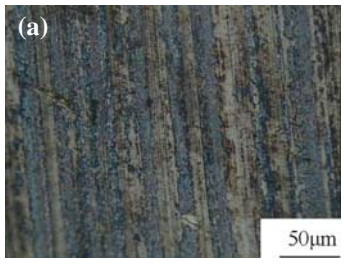

Wear track after running against wooden disc for 50 minutes

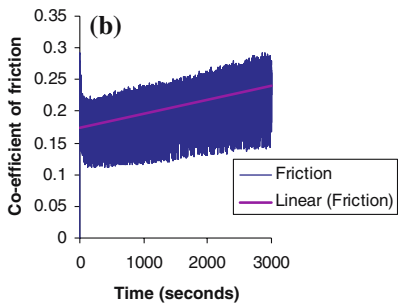

Variation of co-efficient of friction with time

Fig. 11 Wear characteristics of AC7 without SBF. (a) Wear track running against wooden disc for 50 min. (b) Variation of co-efficient of friction with time

Table 6 Results of wear

Coating	Co-efficient of friction (μ)	Specific wear rate ($\times 10^{-12}$ kg/Nm)
AC1	0.17	10.85
AC2	0.19	50.65
AC3	0.20	25.3
AC4	0.20	7.23
AC5	0.20	3.61
AC6	0.20	3.61
AC7	0.20	3.61

surfaces (at a level that allows vascular in-growth) will encourage bone ingrowth/apposition [21] and provide good bone screw fixation [22]. However, a very rough surface will have more particulate concentration around the implant [12]. Therefore, it is reasonable to assume that AC6 and AC7 which have low specific wear rate but very rough surface would provide more wear debris concentrated around the implant and cause pain to the patient. But AC5 has low specific wear rate and smooth surface and it is believed to produce less debris around the implant inside the body. The coatings produced from shorter duration have high specific wear rates and their implantation may not offer any advantage to the patients.

To summarise, coating AC4 shows amorphous regions in TEM and contains self-healing pores. It offers good resistance to uniform corrosion by SBF and has low specific wear rate. Coating AC5 was produced by treating for 10 h and contains more phosphorus than all other coatings. It offers good resistance to uniform corrosion by SBF and has the lowest specific wear rate. Coating AC7, produced by treatment for 24 h has low thickness. It has poor impedance in the SBF medium and lowest specific wear rate.

7 Conclusion

Of all the coatings reported in this paper, coating AC5, which is obtained by anodising Ti–6Al–4V at a current density of 10 mA/cm^2 for 10 h, has the best combination of corrosion properties in SBF and wear against wooden disc and hence is recommended as a suitable candidate for implant material.

References

1. A. BIGI, E. BOANINI, B. BRACCI, A. FACCHINI, S. PANZAVOLTA, F. SEGATTI, L. STURBA, *Biomaterials* **26** (2005) 4085
2. H. ISHIZAWA, M. OGINO, *J. Biomed. Mater. Res.* **29** (1995) 65
3. M. SHIRKHANZADEH, *J. Mater. Sci.: Mater. Med.* **3** (1992) 322
4. M. LONG, H. J. RACK, *Biomaterials* **19** (1998) 1621
5. M. A. ARENAS, T. J. TATE, A. CONDE, J. DE DAMBORENA, *Br. Corrosion J.* **35** (2000) 232
6. A. CIGADA, M. CABRINI, P. PEDEFERRI, *J. Mater. Sci.: Mater. Med.* **3** (1992) 408
7. S. FERDJANI, D. DAVID, G. BERANGER, *J. Alloy Compd.* **200** (1993) 191
8. A. MONTENERO, G. GNAPPI, F. FERRARI, M. CESARI, E. SALVIOLI, L. MATTOGNO, S. KACIULIS, M. FINI, *J. Mater. Sci.* **15** (2000) 2791
9. L. AGATA DE SENA, M. CALIXTO DE ANDRADE, A. MALTA ROSSI, G. DE ALMEIDA SOARES, *J. Biomed. Mater. Res.* **60** (2002) 1
10. M. F. MAITZ, M. T. PHAM, W. MATZ, H. REUTHER, G. STEINER, *Surf. Coat. Technol.* **158–159** (2002) 151
11. H. ISHIZAWA, M. OGINO, *J. Biomed. Mater. Res.* **29** (1995) 1071
12. K. A. GROSS, M. BABOVIC, *Biomaterials* **23** (2002) 4731
13. M. POURBAIX, 1963, Atlas d'quilibre electrochimique à 25° (Paris: Gauthier-Villars & Cie)
14. J. BASZKIEWICZ, D. KRUPA, J. A. KOZUBOWSKI, B. RAJCHEL, M. MITURA, A. BARCZ, A. SLÓSARCZYK, Z. PASZKIEWICZ, Z. PUFF, *Vacuum* **70** (2003) 163
15. J. LAUSMAA, B. KASEMO, H. MATTSSON, H. ODELIUS, *Appl. Surf. Sci.* **45** (1990) 189
16. J. PAN, D. THIERRY, C. LEYGRAF, *Electrochim. Acta* **41** (1996) 1143
17. C. FONSECA, M. A. BARBOSA, *Corrosion Sci.* **43** (2001) 547
18. D. VELTEN, V. BIEHL, F. AUBERTIN, B. VALESKE, W. POSSART, J. BREME, *J. Biomed. Mater. Res.* **59** (2002) 18
19. I. MILOŠEV, M. METIKOS-HUKOVIC, H.-H. STREHBLOW, *Biomaterials* **21** (2000) 2103
20. M. F. LOPEZ, A. GUTIERREZ, J. A. JIMENEZ, *Electrochim. Acta* **47** (2002) 1359
21. H. MARCELO, P. DA SILVA, G. D. A. SOARES, C. N. ELIAS, S. M. BEST, I. R. GIBSON, L. DISILVIO, M. J. DALBY, *J. Mater. Sci.: Mater. Med.* **14** (2003) 511
22. G. MAGYAR, S. TOKSVIGLARSEN, A. MORONI, *J. Bone Joint Surg.* **79B** (1997) 487